Huang LW, Elkedim O. Mg-Ni-based systems for hydrogen storage. Chapter to be published in Handbook of Nanomaterials for Hydrogen Storage.

Mg-Ni-based systems for hydrogen storage

L.W. Huang [a,*], O. Elkedim [a,*]

[a] FEMTO-ST, MN2S, Université de Technologie de Belfort-Montbéliard, Site de Sévenans, 90010 Belfort cedex, France

[*]Corresponding author. Tel.: + 33 3 84583545 ; Fax: + 33 3 84583000

E-mail address: liwu.huang@utbm.fr (L.W. Huang); omar.elkedim@utbm.fr (O. Elkedim)

1. Introduction

Mg-Ni-based alloys are considered to be promising candidates for hydrogen storage applications because of their low cost, light weight and rich mineral resources, as well as high theoretical hydrogen storage capacity (assuming the formation of Mg_2NiH_4, it is 3.6 mass%, equivalent to 999 mAh/g for the discharge capacity, which is approximately 2.7 times that of $LaNi_5$ [1]). However, the high thermodynamical stability, sluggish hydriding/dehydriding kinetics and poor cycle stability of Mg-Ni-based alloys become the obstacle for the practical use for hydrogen storage.

In this chapter, firstly, the fundamental data on Mg-Ni-based systems and their hydrides are briefly summarized, including phase diagrams, crystal structures and thermodynamical properties etc. Meantime, the phase compositions of Mg-Ni-based alloys, especially nanostructured and amorphous phases are discussed. Secondly, the methods of improving hydrogen storage properties of Mg-Ni-based systems, such as (1) partial element substitution; (2) adding suitable catalysts; (3) adding carbon materials; (4) different preparing methods for synthesizing Mg-Ni-based alloys, are presented. Thirdly, first principles investigation on Mg-Ni-based alloys (including substitutional doping of other elements) and their hydrides (e.g. high temperature (HT)-Mg_2NiH_4 and low temperature (LT)-Mg_2NiH_4) is discussed. Finally, the conclusions are given.

2. Fundamental data of Mg_2Ni and its hydrides

Fig.1 shows the Mg-Ni binary phase diagram, and it can be seen that there are two stable compounds, namely $MgNi_2$ and Mg_2Ni. $MgNi_2$ does not react with H_2 at pressures up to 27.6 bar and temperatures up to 350℃. Whereas, Mg_2Ni reacts readily with H_2 at 20.7 bar and 325℃ [2].

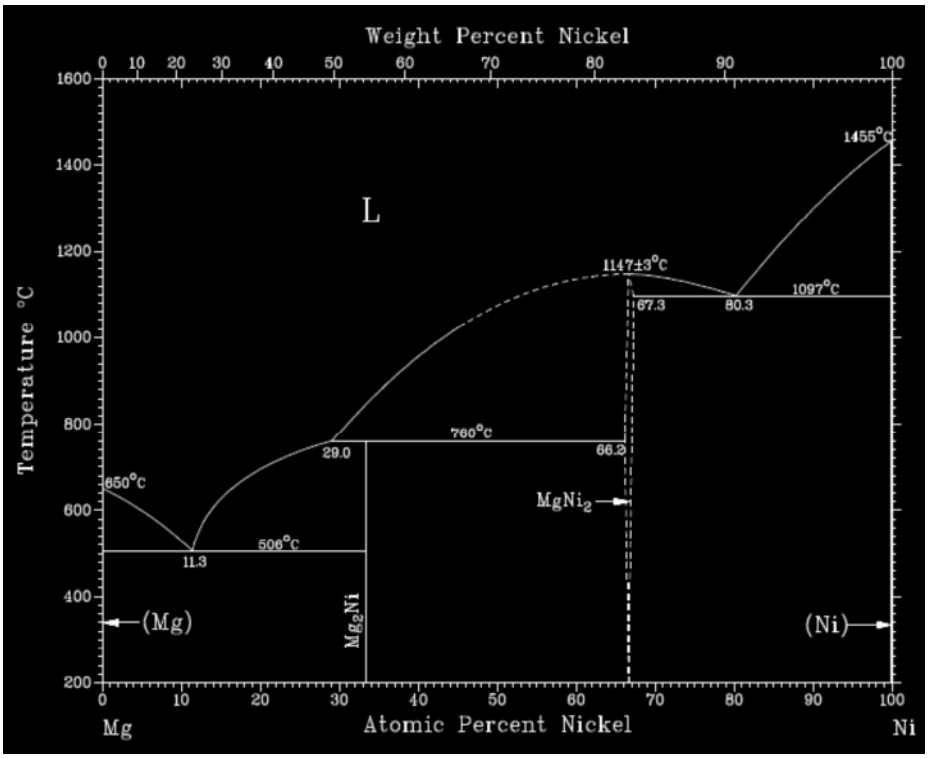

Fig. 1 Mg-Ni binary phase diagram [4]

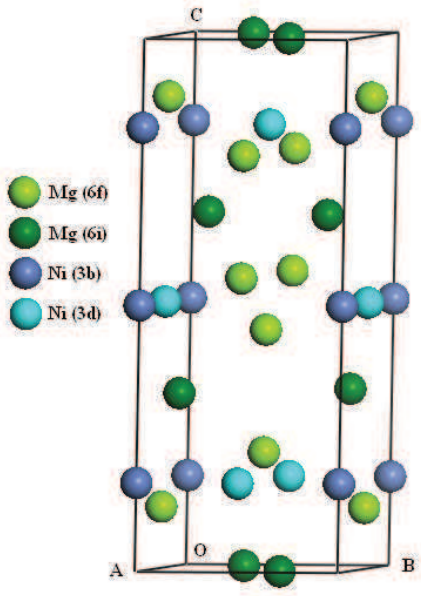

Fig. 2 Models of the unit cell of Mg_2Ni

The structure of Mg_2Ni phase is shown in Fig. 2. Its unit cell belongs to the space group $P6_222$ with lattice parameters a=5.216(6) Å, c=13.20(6) Å [3]. The Mg_2Ni unit cell contains 6 formula units, and therefore it can be expressed as $Mg_{12}Ni_6$. The 12 Mg atoms occupy *6f* and *6i* lattice sites, while 6 Ni atoms occupy *3b* and *3d* lattice sites. The different lattice sites are denoted by the balls in different colors as shown in Fig.2.

Upon hydrogenation, in the first stage, hydrogen dissolves in the Mg_2Ni phase to the extent that the ratio of H/(Mg + Ni)≅0.1 according to the reaction (1.1)

$$Mg_2Ni+0.15H_2 \rightleftarrows Mg_2NiH_{0.3} \quad (1.1)$$

When hydrogen is absorbed by Mg_2Ni beyond 0.3 H per unit formula, the system undergoes a structural rearrangement to the stoichiometric complex hydride Mg_2NiH_4 according to the reaction (1.2)

$$0.54Mg_2NiH_{0.3}+H_2 \rightleftarrows 0.54Mg_2NiH_4 \quad (1.2)$$

In a word, Mg_2Ni reacts with hydrogen to form the hydride phase Mg_2NiH_4 according the reversible reaction (1.3)

$$Mg_2Ni+2H_2 \rightleftarrows Mg_2NiH_4 \quad (1.3)$$

Therefore the theoretical gravimetric hydrogen storage capacity of Mg_2Ni alloy is 3.6%. Additionally, metastable oversaturated phases, such as Mg_2NiH [5], $Mg_2NiH_{1.2}$ [6] and $Mg_2NiH_{1.8}$ [7] have also been reported. Mg_2NiH_4 hydride has two polymorphs: low temperature (LT)-Mg_2NiH_4 (monoclinic) and high temperature (HT)-Mg_2NiH_4 (cubic). The transition temperature is between 210 and 240℃ [8]. The unit cells of these two polymorphs are exhibited in Fig. 3. It can be seen from Fig. 3a that the LT phase has monoclinic symmetry with space group *C2/c* (*a* = 14.343 (5) Å, *b* = 6.4038 (10) Å, *c* = 6.4830 (13) Å, *β* = 113.52 (4)°) [8]. The monoclinic Mg_2NiH_4 unit cell contains 8 formula units, which can be expressed as $Mg_{16}Ni_8H_{32}$. It contains four types of symmetry-independent H atoms (*8f*), which surround Ni atoms (*8f*) in nearly regular tetrahedral configurations. The unit cell of the HT-Mg_2NiH_4 is shown in Fig. 3b. Its unit cell belongs to the space group *Fm-3m* with lattice parameter *a*= 6.507 (2)

Å [9]. The metal atoms exhibit an anti-fluorite arrangement. Ni and Mg atoms occupy the cation (*4a*) and anion (*8c*) sites, respectively, whereas the H distribution has not been completely determined by diffraction methods. García et al [10] calculated the electronic properties of cubic Mg_2NiH_4 for different hydrogen configurations and concluded that the minimum-energy configuration corresponds to a tetrahedrally distorted square-planar distribution of hydrogen atoms around the nickel atom. They also indicated that the regular tetrahedral arrangement as shown in Fig. 3b produced a semiconductor with an indirect gap of 1.17eV, which is in agreement with experimental results [11]. In both HT and LT-Mg_2NiH_4, the bonding interaction between Ni and H is stronger than that between Mg and H, and hydrogen is bonded with nickel in a mixed ionic–covalent bonding to form a complex $[NiH_4]^{4-}$ which in turn bonds ionically to the Mg^{2+} ions.

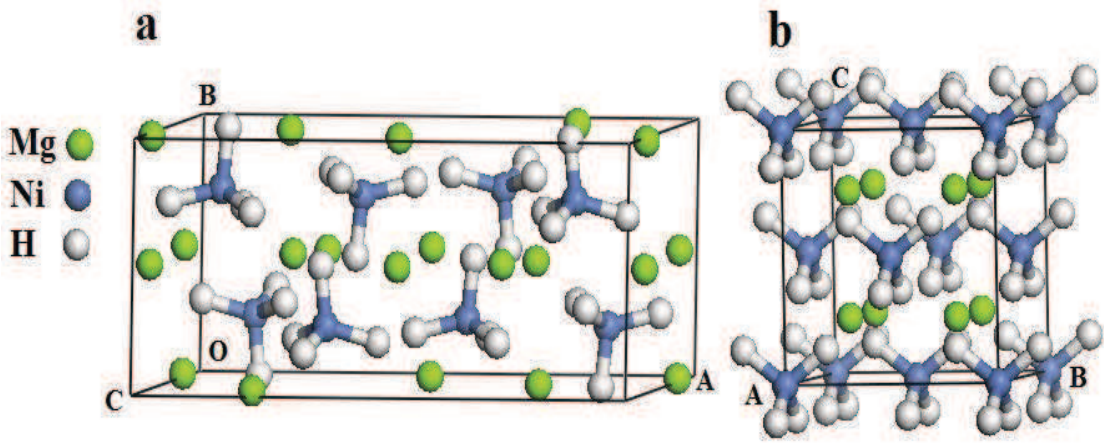

Fig. 3 Models of the unit cells of LT-Mg_2NiH_4 (a) and HT-Mg_2NiH_4 (b)

Though Mg_2NiH_4 possesses a high hydrogen storage capacity, it is too stable in terms of thermodynamics (requiring 280℃ for 1bar hydrogen [12]). The enthalpy of formation of Mg_2NiH_4 is −64.5 kJ/mol H_2 [2], whereas the attractive enthalpy change for hydrogen storage is between 30 and 48 kJ/mol H_2 [12]. Therefore, its thermodynamic property should be improved at first in order to launch it into practical application for hydrogen storage.

3. Amorphous and nanostructured phases of Mg-Ni-based systems

The hydrogen storage properties of conventional polycrystalline Mg_2Ni are rather poor, and therefore amorphous and nanocrystalline phases of Mg-Ni-based systems are often introduced for improving the hydrogen storage properties.

Amorphous structures, metastable in terms of thermodynamics, differ from the equilibrium, crystalline state essentially in the local configuration of atoms. The lack of a crystallographically defined structural unit results in a distribution of local atomic positions in the structure of the glass. As a consequence, amorphous structure can provide a wide distribution of the available sites for hydrogen [13-15]. Therefore, the hydrogenation behaviour of the amorphous structure is totally different from that of the thermodynamically stable, crystalline material, although both materials may have identical composition. The results of the high-resolution ^{1}H-NMR measurements [16] also indicated that the local environment of hydrogen in amorphous MgNi exhibited an intermediate character between those in Mg_2NiH_4 with stable mixed ionic–covalent bonding and in $Mg_2NiH_{0.3}$ with weak metallic bonding of hydrogen solution. Orimo and Fujii [17] indicated that the dehydriding temperature of amorphous MgNi under argon was lower than that of conventional Mg_2NiH_4.

Nanocrystalline metals are different in microstructure from both polycrystalline and amorphous phases. Because of the reduction of crystallite size, the large number of interfaces and grain boundaries are produced, which can enhance the solubility and provide easier channel for the diffusion of hydrogen atoms, avoiding the long-range diffusion of hydrogen through an already formed hydride. It has been reported that the introduction of nanocrystalline Mg_2Ni decreased the dehydriding temperature of Mg_2NiH_4 [17].

It is worthy to point out that, amorphous and nanocrystalline phases often coexist and the nanocrystallites are embedded in the amorphous matrix. This microstructure characteristic is favourable for the hydrogen storage [18], which may be explained by an interaction between the amorphous regions of grain boundaries and the nano-grains. The amorphous region is hydrogenated first, expands and so puts the encased nano-grains under pressure, thus showing synergistic effects on the hydrogen storage properties of Mg_2Ni-type alloy. Orimo and Fujii [17] reported that the maximum hydrogen concentrations of the three regions had been experimentally determined to be 0.3% in the grain region of nanocrystalline Mg_2Ni, 4.0% in the interface between Mg_2Ni grains and 2.2% in the amorphous region. Yamamoto et al [19] studied the formation process of amorphous MgNi by milling Mg_2Ni and Ni powders. Fig. 4 exhibits the schematic illustrations of the formation process of amorphous MgNi phase. As shown in Fig. 4a, the nanocrystalline Mg_2Ni consists of the Mg_2Ni nanocrystals (intra-grain) and surrounding disordered region (inter-grain). In Fig. 4b, Ni is kneaded in the extremely thin plates and stacks together with nanocrystalline

Mg_2Ni. Kneaded Ni metal reacts with the inter-grain region to form amorphous phase at the interfaces. Finally, metastable amorphous phase of MgNi is completely formed as shown in Fig. 4c.

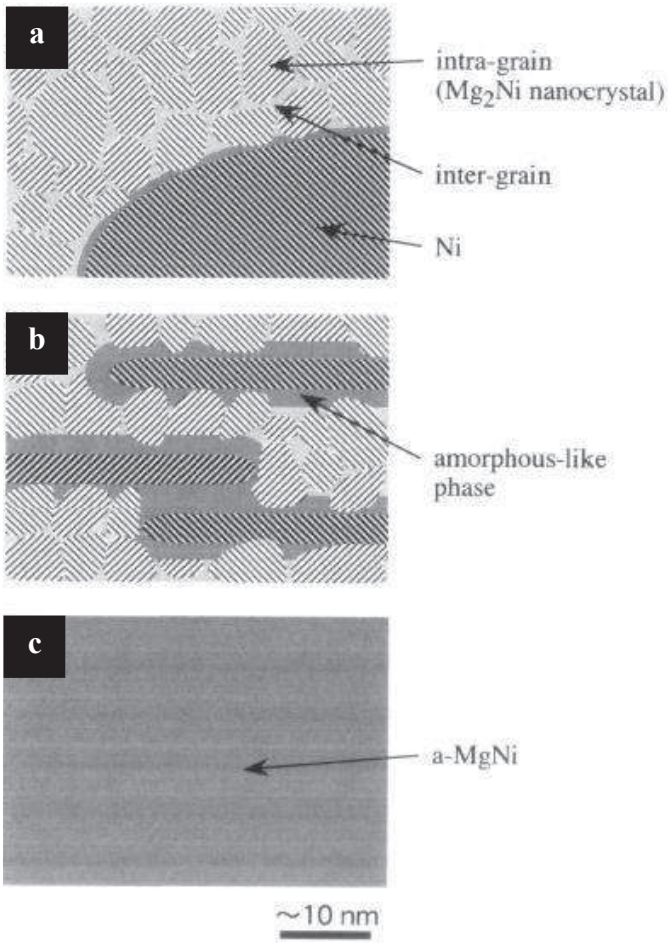

Fig. 4 Schematic illustrations of the formation process of amorphous-MgNi phase during mechanical alloying [19]

4. Methods of improving hydrogen storage properties of Mg-Ni-based systems

4.1. Partial element substitution

Partial element substitution could change the composition of milled alloys and even introduces new phases. Therefore, this method has been widely used to improving hydrogen storage properties of Mg-Ni-based alloys.

4.1.1. Substitution for Mg

Al. The partial substitution of Al for Mg could result in the formation of Al_2O_3

protective film on the surface of matrix alloy. The Al_2O_3 plays a role of an inhibitor against further corrosion of the alloy. Therefore, the partial substitution of Al for Mg can prolong the cycle life of Mg_2Ni alloy [20]. Wang et al [21] synthesized $Mg_{2-x}Al_xNi$ ($0 \leq x \leq 0.6$) series alloys by interdiffusing Mg, Ni and Al powders together and investigated the effects of partial substitution of Al for Mg on the structure and electrochemical performance. They found that a new compound, Mg_3AlNi_2 was formed and the electrochemical capacity and cycle life of alloy electrodes increased markedly with increasing amount of this new compound in alloys. The alloys containing this new compound presented excellent electrochemical performance. Mg_3AlNi_2 is first reported to be synthesized by Lü et al [22]. It belongs to *Fd-3m* with a cell parameter a=1.15474(2) nm and Z= 16. Its unit cell is shown in Fig. 5. Mg_3AlNi_2 is considered to be a promising hydrogen storage material for future use in hydrogen storage systems and Ni–MH batteries.

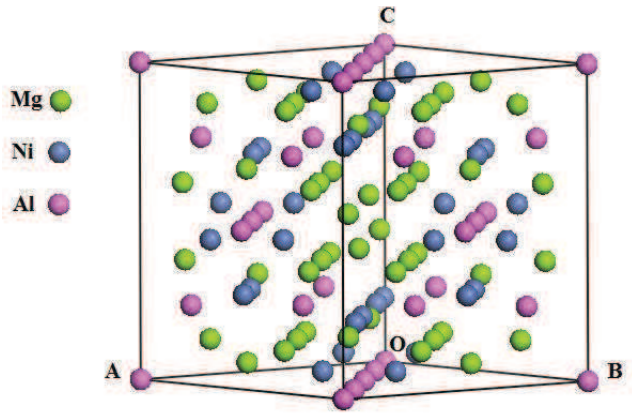

Fig. 5 Model of the unit cell of Mg_3AlNi_2

Ti. Partial substitution of Mg by Ti could reduce the activation energy of desorption from 69 kJ mol^{-1} for nanocrystalline Mg_2Ni to 59 kJ mol^{-1} for $Mg_{1.9}Ti_{0.1}Ni$ and therefore destabilized the hydride phase. [23]. Additionally, Ti substitution for Mg could improve cycle stability of Mg–Ni-Ti ternary alloys due to the formation of TiO_2 that limited $Mg(OH)_2$ formation [24] Finally, the partial substitution of Mg by Ti in Mg-Ni-based system can introduce new phases, such as TiNi, Ti_2Ni and $TiNi_3$. Composite phase structure is favorable for improving the hydrogen storage properties of Mg-Ni-based system.

Zr. Zhang et al [25] prepared electrode alloys $Mg_{2-x}Zr_xNi$ (x = 0, 0.15, 0.3, 0.45 and 0.6) by mechanical alloying. They indicated that the substitution of Zr was favourable for the formation of an amorphous phase. For a fixed milling time, the

amorphous phase in the alloy grew with increasing Zr content. The substitution of Zr could dramatically enhance the discharge capacity with preferable cycle stability, and improved the discharge voltage characteristic of the alloys.

V. The partial substitution of Mg in MgNi with V could suppress the formation of $Mg(OH)_2$ on the alloy surface during the charge–discharge cycling in alkaline solution [26] and therefore improves cycle life of MgNi alloy.

Combined Ti and Zr. Anik et al [27] investigated $Mg_{1.5}Ti_{0.5-x}Zr_xNi$ (x = 0, 0.1, 0.2, 0.3, 0.4) alloys synthesized by mechanical alloying and their electrochemical hydrogen storage characteristics. They found that the replacement elements Ti and Zr perfectly dissolved in the amorphous phase and Zr facilitated the amorphization of the alloys. The presence of Zr in the Ti-including Mg-based alloys improved the cyclic stability of the alloys. This action of Zr was attributed to the less stable and more porous characteristics of the barrier hydroxide layer in the presence of Zr due to the selective dissolution of the disseminated Zr-oxides throughout the hydroxide layer on the alloy surface. Zhang et al [28] also obtained a similar conclusion. In a word, the corrosion inhibiting effect of Zr alone, without the presence of Ti was weak. The synergetic effect of Zr and Ti made the alloys more protective than by Ti or Zr alone.

Combined Ti and V. Iwakura et al [29] studied $Mg_{0.9}Ti_{0.06}V_{0.04}Ni$ alloys prepared by mechanical alloying (MA). They indicated that the oxidation of Mg on the alloy surface during the charge–discharge cycles could be fairly suppressed by the partial substitution with both Ti and V. Moreover, it was found from Auger electron spectroscopy (AES) that thickness of oxidized surface layer of the MgNi alloy particle was decreased by the introduction of both Ti and V. It was suggested that composite oxide layer in which both Ti and V species existed might be very effective in suppressing the oxidation of the alloy surface, leading to the synergistic effect on charge–discharge cycle performance.

Mn. The partial substitution of Mg by Mn in Mg_2Ni alloy can enhance the discharge capacity of Mg_2Ni alloy at room temperature [30, 31]. Kohno et al. [32] reported that as a result of substitution of Mg with Mn, absorption of hydrogen occurred at lower temperature.

La. Ren et al [33] prepared alloys $Mg_{20-x}La_xNi_{10}$ (x = 0, 2, 4, 6) by casting and rapid quenching. The substitution of La for Mg significantly enhanced the glass

forming ability of the alloys. La significantly improved the cycle stability of the as-cast and the quenched alloys. For as-cast alloys, the hydrogen absorption and desorption capacities and kinetics clearly rose with increasing La content. For as-quenched alloy, when La content x = 2, it displayed an optimal hydrogen desorption kinetics at 200 °C. Additionally, the discharge capacities of the as-cast alloys rose with the increase of La content, but those of the as-quenched alloys obtained the maximum values with the variation of La content.

Sn. Drenchev et al [34] studied the electrochemical hydriding/dehydriding of nanostructured $Mg_{2-x}Sn_xNi$ (x = 0, 0.1, 0.3). Sn addition could decrease the electron density around the Mg atoms and therefore impedes magnesium oxidation. As a result, the cycle life of Mg_2Ni can be essentially improved. Moreover, though Sn hampers charge transfer, it could lower the hydrogen diffusion resistance in Mg_2Ni based alloys.

Ag. Li et al [35] studied the $Mg_{2-x}Ag_xNi$ alloys and found that partial substitution of Ag for Mg leaded to a faster rate of hydriding. Thus, Ag substitution could improve the hydriding kinetics of Mg_2Ni alloy.

Cr. Xue et al [36] produce a series of $Mg_{2-x}Cr_xNi$ alloy powder by combination of solid-state diffusion with mechanical grinding. It was found that partial replacement of Mg by Cr could increase the mass discharge capacity and improve the cycle life of Mg_2Ni alloy.

4.1.2. Substitution for Ni

Mn. We have investigated the structure and electrochemical hydrogen storage properties of $Mg_2Ni_{1-x}Mn_x$ (x=0, 0.125, 0.25, 0.375) alloys prepared by mechanical alloying. We concluded that it was difficult for Mn to substitute Ni site in Mg_2Ni lattice structure and the substitution of Mn for Ni could inhibit the formation of $MgNi_2$ phase. It is worthy to point out that we have synthesized Mg_3MnNi_2 by a much simpler one-step technique which was milling elemental powders of Mg, Ni and Mn in argon atmosphere [18]. Mg_3MnNi_2 phase was relatively stable during charge/discharge cycles and therefore could significantly enhance the cycle stability under simultaneously maintaining a high discharge capacity. Three other preparing methods have also been reported to synthesize the Mg_3MnNi_2 alloy. Denys et al. [37] synthesized Mg_3MnNi_2 intermetallic compound by high-energy ball milling in argon

atmosphere with subsequent pressing and sintering. They found that the synthesized Mg_3MnNi_2 phase exhibited an ideal electrochemical discharge curve and good cyclic stability in comparison with other magnesium alloys. Dobrovolsky et al. [39] obtained Mg_3MnNi_2 using milling a mixture of Mg, Ni and Mn powders in hydrogen atmosphere followed by thermal decomposition of the MA product. Hsu et al. [39] prepared Mg_3MnNi_2 alloy by the method integrating conventional melting and isothermal evaporation casting process (IECP).

Mg_3MnNi_2 phase, as a new hydrogen storage alloy, has shown better hydrogen storage properties. The unit cell of Mg_3MnNi_2 phase is shown in Fig. 6. It has a cubic symmetry (space group *Fd-3m*) with the lattice parameter a=11.564 Å [40]. Each unit cell contains 16 formula units of Mg_3MnNi_2, namely $Mg_{48}Mn_{16}Ni_{32}$. 48 Mg atoms, 16 Mn atoms and 32 Ni atoms occupy Mg (*48f*), Mn (*16d*) and Ni (*32e*) lattice sites, respectively. H atoms can partially fill *16d* Mg_6 octahedral and *32e* Mg_3Ni tetrahedral interstices in the cubic metal matrix as shown in Fig. 7 [41].

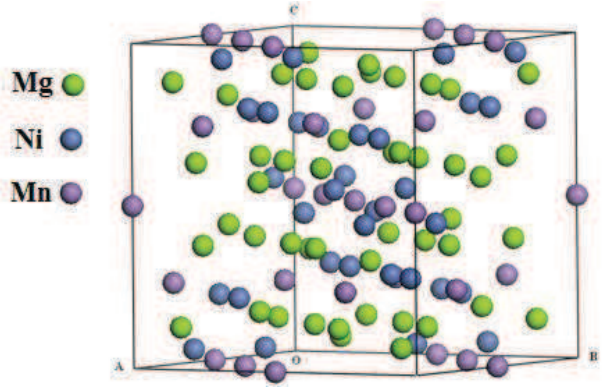

Fig. 6 Model of the unit cell of Mg_3MnNi_2

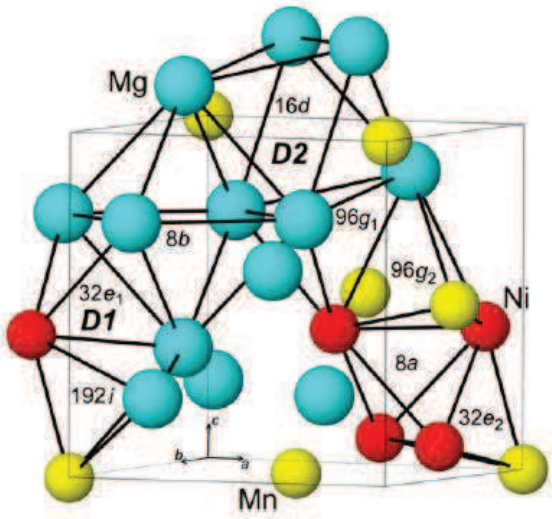

Fig. 7 Types of interstices in the structure of Mg_3MnNi_2 [41]

Cu. Zhang et al [42] synthesized the nanocrystalline Mg_2Ni-type alloys with nominal compositions of $Mg_{20}Ni_{10-x}Cu_x$ (x = 0–4) by melt-spinning technique. They indicated that the substitution of Cu for Ni enlarged cell volume, led to a significant refinement of the grains and the formation of the secondary phase Mg_2Cu, as well as weakened stability of the hydride in the as-cast alloys. Therefore, the substitution of Cu for Ni could enhance the discharge capacity and the electrochemical cycle stability of nanocrystalline Mg_2Ni-type alloys.

Co. Similar to Zr, the substitution of Co for Ni could significantly heighten the glass forming ability of the Mg_2Ni-type alloy [43]. The substitution of Co for Ni does not change the major phase of Mg_2Ni, but it leads to the formation of secondary phase $MgCo_2$. Zhang et al [43] indicated that the secondary phase $MgCo_2$ probably worked as a catalyst to activate the Mg_2Ni phase to absorb/desorb reversibly hydrogen in the alkaline electrolyte. As a result, the maximum discharge capacity and the capacity retaining rate of Mg_2Ni-type alloy can be improved by Co substitution.

4.1.3. Simultaneous substitution for Mg and Ni

Wang et al [44] studied the quaternary $Mg_{1.75}Al_{0.25}Ni_{0.9}M_{0.1}$ (M=Cr, Fe and Co; $0 \leq x \leq 0.3$) alloys prepared by means of solid diffusion method. They found that Mg_3AlNi_2 was the main phase in the quaternary alloys as that of ternary $Mg_{1.75}Al_{0.25}Ni$ alloy. Due to the Cr, Fe or Co substitution, the quaternary alloy showed larger discharge capacity and higher cycling stability than the $Mg_{1.75}Al_{0.25}Ni$ ternary alloy, which could be attributed to the fact that the additional Cr, Fe and Co could effectively improve the reaction activity of electrode.

4.2. Adding appropriate catalysts

The sluggish hydriding/dehydriding kinetics of Mg-Ni-based alloys is an obstacle for the practical application for hydrogen storage. Adding suitable catalysts can improve the hydriding/dehydriding kinetics.

The mechanism of the catalysis may be caused by a spillover effect. The hydrogen spillover phenomenon is defined as dissociative chemisorption of H_2 on a metal and subsequent migration or surface diffusion of the atomic hydrogen onto the support surfaces [45, 46]. Spillover effect has long been observed on supported metal catalysts. For catalytic hydrogen absorption and release, the catalyst particles should

preferably be deposited on the outer surface of the alloy particles to ensure the best catalytic effect [47]. If the catalyst particles are capsulated in the alloy particles, hydrogen molecules cannot contact with the catalyst and the "catalyst" has no promotional effect for hydrogen absorption. Gutfleisch et al [48] found that co-milling Mg_2Ni with Ru for a short time, such as 1 h, made the onset temperature of hydrogen desorption be decreased as low as 80 °C. However Co-milling the nanocrystalline hydride with platinum group metals (PGM) catalysts for long durations made the catalysts diffuse into the bulk and consequently destroyed its effectiveness at the surface. Moreover, the coating of Mg_2Ni-type hydrides with the PGM catalyst could protect the surface from oxidation, which led to an improved cycle stability.

Pd is one of the most important catalysts used to improve the the hydriding/dehydriding kinetics of Mg-Ni-based alloys. Zaluski et al [49] prepared nanocrystalline Mg_2Ni by ball milling and small amounts of Pd (less than 1 wt. %) were added for the catalytic modification of the surface of the Mg_2Ni powder. They concluded that the powders modified with Pd showed substantially enhanced hydrogen absorption kinetics and were much less sensitive to air exposures, which normally poisoned the surface and created a barrier for hydrogen dissociation and transfer into the material. Spillover mechanism can be used to explain the catalytic effect of palladium. The Pd catalyst acted effectively when present in the form of small clusters or particles dispersed on the surface of the absorbing material.

Xu et al [50] deposited nano-particles of various metal catalysts (palladium, platinum and ruthenium) on the outer surface of magnesium powders through a wet chemistry process. As a result, both the hydrogen absorption and hydrogen release kinetics of magnesium were significantly improved by doping the nano-particle catalysts. Palladium showed the best catalytic effect among the three metals-doped and examined. Doping 0.5 mol % nano-particle palladium made the hydrogen absorption and hydrogen release rates of magnesium increase 1 and 14 times, respectively. The added nano-particle palladium probably acts as hydrogen pumps, during the desorption process and consequently leads to a faster hydrogen release.

4.3. Adding carbon materials

Carbon materials exhibit certain properties that make them in combination with metal hydrides more suitable compared to other potential supports or additives [51]. Generally speaking, all of the carbon allotropes, such as graphite, fullerene, activated

carbon, carbon black and carbon nanotubes (CNTs), show positive effects on the hydrogen storage properties of Mg-based systems. It has been reported that the addition of graphite, fullerene or Vulcan carbon black in small amounts (5 wt. %) to nanocrystalline Mg_2Ni could increase the desorption kinetics of Mg_2Ni [52]. Wu et al. [53] have studied the effect of various carbon additives and noncarbon materials on hydrogen capacity and dehydriding/hydriding kinetics of Mg. Interestingly, all the carbon additives exhibited prominent advantage over the noncarbon additives and among the various carbon additives, purified single-walled carbon nanotubes (SWCNTs) exhibited the most prominent "catalytic" effect on improving hydrogen capacity, absorption/desorption kinetics of Mg. Quite recently, Amirkhiz et al. [54] reported that the coupled additions of SWCNTs and metallic nanoparticles could catalyze the desorption of hydrogen for MgH_2 powders. This research group [55] also studied the hydrogen sorption cycling performance of SWCNTs-Mg hydride nanocomposites and indicated that the nanocomposites displayed much improved kinetic stability relative to MgH_2. Besides SWCNT, multiwalled carbon nanotube (MWCNT) has also been reported to be an excellent additive for improving hydrogen storage properties of Mg-based systems. Pandey et al. [56] investigated the admixing of MWCNTs in Mg_2Ni and Aminorroaya et al. [57] studied the co-milling of MWCNTs and Mg-6 wt. % Ni alloy. They indicated that MWCNTs were very effective at promoting the desorption kinetics and increasing the hydrogen capacity of these alloys. Recently, Verón et al. [58] reported that coupled addition of Co and MWCNTs showed synergetic effect on hydrogen sorption properties of MgH_2. Therefore, integrating the advantages of both metal substitution and MWCNTs addition to improve electrochemical hydrogen storage properties of Mg_2Ni-type alloy is an open subject.

We have prepared $Mg_{2-x}Al_xNi$ (x = 0, 0.25) electrode alloys with and without multiwalled carbon nanotubes (MWCNTs) by mechanical alloying under argon atmosphere at room temperature using a planetary high energy ball mill [59]. Al substitution resulted in the formation of AlNi-type solid solution that could interstitially dissolve hydrogen atoms. In contrast, the addition of MWCNTs hardly affects the XRD patterns. After co-milling with 5 wt. % MWCNTs, the particle sizes of both Mg_2Ni and $Mg_{1.75}Al_{0.25}Ni$ milled alloys were decreased explicitly. The TEM images in Fig. 8 reveal that the MWCNTs aggregate along the boundaries and surfaces of milled alloy particles and play a role of lubricant to weaken the adhesion of alloy particles. The majority of MWCNTs retain their tubular structure after ball

milling except a few MWCNTs whose tubular structure is destroyed as shown in Fig. 9. Electrochemical measurements indicate that all milled alloys have excellent activation properties. The $Mg_{1.75}Al_{0.25}Ni$-MWCNTs composite shows the highest discharge capacity due to the synergistic effects of MWCNTs and Al on the electrochemical hydrogen storage properties of Mg_2Ni-type alloy. However, the improvement on the electrode cycle stability by adding MWCNTs is unsatisfactory.

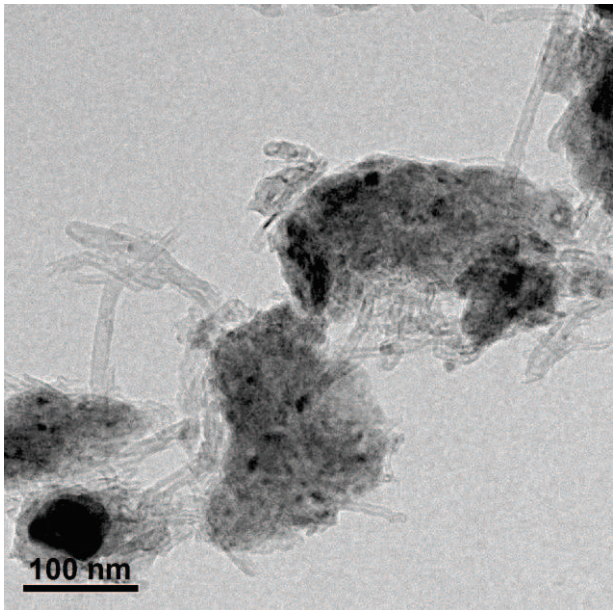

Fig. 8 – Bright field TEM image of milled $Mg_{1.75}Al_{0.25}Ni$-MWCNTs composite [59]

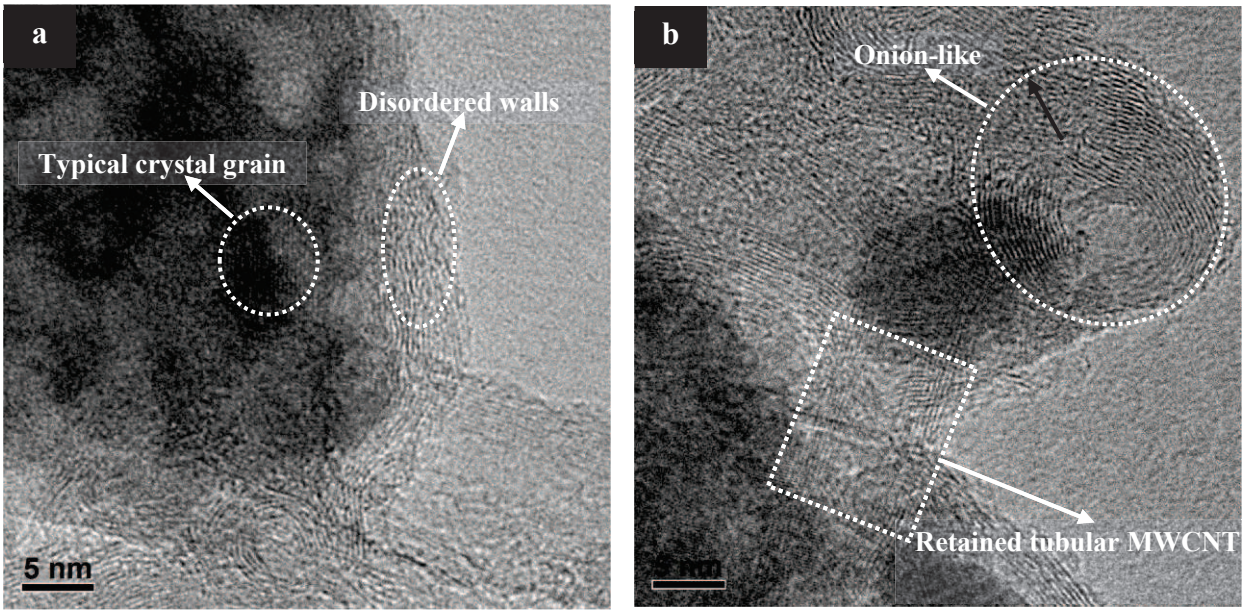

Fig. 9 – HRTEM image of milled $Mg_{1.75}Al_{0.25}Ni$-MWCNTs composite [59].

4.4. Preparing methods

4.4.1. Mechanical alloying

Mechanical alloying is a solid-state powder processing technique involving repeated welding, fracturing, and rewelding of powder particles in a high-energy ball mill [60]. Fig. 10 exhibits the schematic depicting the ball motion inside the ball mill. It can be seen that the vials and the supporting disc rotate in opposite directions and the centrifugal forces alternately act in like and opposite directions. This causes the milling balls to run down the internal wall of the vial – the friction effect, followed by the material being milled and milling balls lifting off and traveling freely through the inner chamber of the vial and colliding against the opposing inside wall – the impact effect [60].

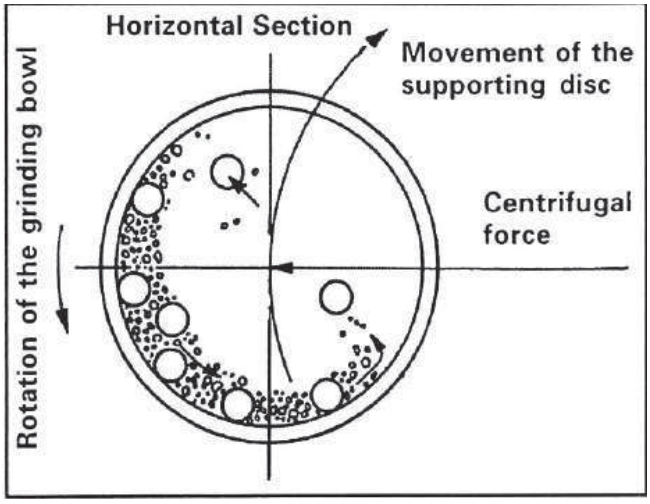

Fig. 10 Schematic depicting the ball motion inside the ball mill [60].

Mechanical alloying is capable of decreasing crystal size, introducing numbers of grain boundaries and defects, as well as facilitating the formation of nanostructured and amorphous phase. The reduction of the average size of the hydriding phase and the increase of the volume fraction of the phase boundary can result in a higher capacity and faster kinetic of hydrogen absorption of Mg-xNi alloys, respectively [61]. Therefore, mechanical alloying is widely used to synthesize Mg-Ni based hydrogen storage alloys. Zaluski et al [62] synthesized nanocrystalline Mg_2Ni by mechanical alloying. This nanocrystalline Mg_2Ni showed hydrogen absorption characteristics superior to that of the conventional crystal phase.

4.4.2. Melt spinning

Fig. 11 shows the working principle of melt spinning [63]. The molten material is driven from the nozzle in the form of a jet and then impinges with the rotating disc to form a melt puddle. Because of a large temperature difference at the melt-substrate interface, the melt beneath the puddle solidifies into a ribbon. Due to the action of the centrifugal force, the ribbon will leave the disc. The cooling rate of the sample can be changed by adjusting the velocity of rotating roller. The melt-spinning technique is the most useful method to obtain an amorphous and/or nanocrystalline phase that could have excellent hydriding characteristics even at room temperature, similar to the alloys produced by the MA process. Zhang et al [64, 65] have synthesized several hydrogen storage alloys containing nanocrystalline phase by melt spinning and this alloys showed improved hydrogen storage properties.

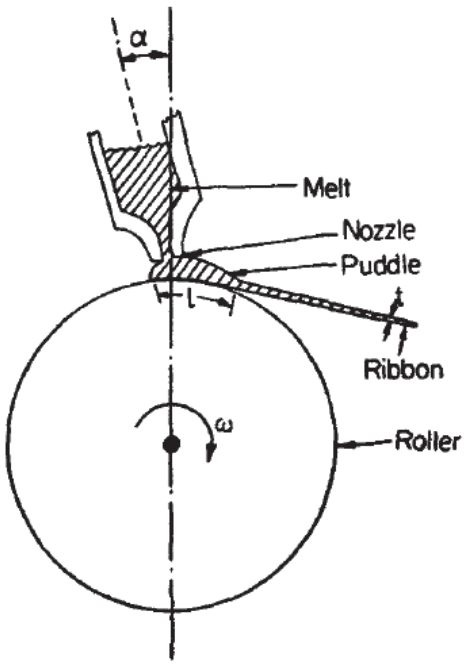

Fig. 11 A schematic diagram of working principle of melt spinning [63]

4.4.3. Combustion synthesis

Combustion synthesis belongs to solid-state combustion reaction without oxygen, in which once one end of the sample is ignited, a highly exothermic reaction can become self-sustaining and yield the final product progressively without any additional heat [66]. Fig. 12 shows a schematic diagram of combustion synthesis. The mixed powders of fine Mg and Ni are compressed. The ignition agent is ignited by a tungsten filament.

The product Mg_2NiH_4 produced by combustion synthesis possesses high activity and excellent hydrogen storage properties: no need of activation process, fast hydriding kinetics and high hydrogen storage capacity [67], which is due to the fact that combustion synthesis could introduce loose and porous morphology, decrease the particle and crystal grain size as well as produce large numbers of fissures on the particle surfaces. As a result, the diffusion of hydrogen inside the particles of alloy and into the crystal grains is enhanced. Recently, combustion synthesis and mechanical alloying have been combined to prepare Mg-Ni-based hydrogen storage alloys and the product exhibited fast kinetics [68, 69].

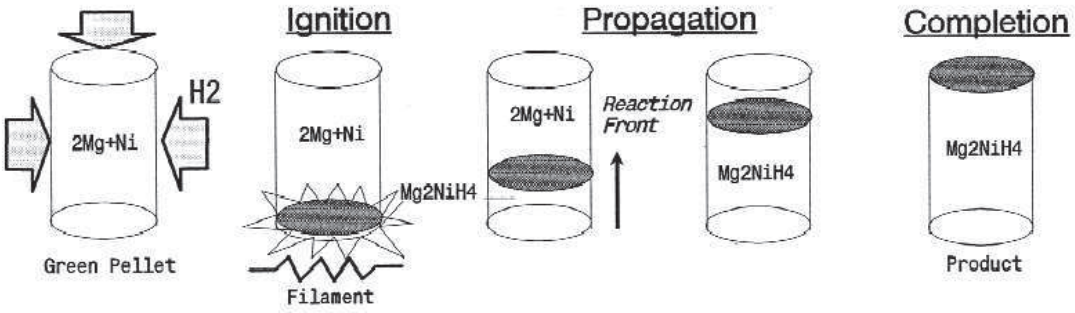

Fig. 12 A schematic diagram of combustion synthesis [66].

4.4.4. Chemical synthetic method

Ikeda and Ohmori [70] prepared Mg_2Ni hydrogen absorbing alloy by chemical synthetic method. The procedure is as follows: at first, Mg particle is immersed in an organic solvent containing Ni ions and the solution is stirred. By this procedure Ni is deposited on Mg. And then the Ni-deposited Mg is heated to obtain Mg_2Ni alloy. Chemical synthetic method is advantageous in that various preparation parameters such as solvent, amount and type of Mg and Ni source, stirring and heating conditions etc. can be controlled for attaining better hydrogen absorption performance.

4.4.5. Polyol reduction

Kumar et al [71] used polyol reduction method followed by annealing to synthesize nanosized Mg_2Ni alloy particles, which showed promising hydrogen absorption as well as electrochemical hydrogen absorption characteristics. The main procedure is: magnesium acetate and nickel acetate are dissolved in ethylene glycol with 2:1 mol ratio. The polyvinylpyrrolidone and the $PdCl_2$ are added, in which Pd acts as a nucleating agent for the growth of nanoparticles of Mg and Ni metals. Then the product is washed and centrifuged. Finally, the as synthesized Mg-Ni alloy is dried in

vacuum followed by annealing in hydrogen atmosphere. The advantage of this method lies in that it gives the flexibility to synthesize uniform size nanoparticles in desired composition range by adjusting the preparation conditions such as reducing agent, protecting reagent concentration, temperature and reaction time.

5. First principles calculations

First principles density functional theory (DFT) calculations can provide fundamental information and are quite helpful to predict and interpret the hydrogen storage properties of materials. Wagemans et al [72] calculated the energies of Mg and MgH_2 clusters of up to 56 Mg atoms with Hartree-Fock and density functional theory methods. They concluded that small MgH_2 clusters had a much lower desorption energy than bulk MgH_2, hence enabling hydrogen desorption at lower temperatures. For instance, an MgH_2 crystallite size of 0.9 nm corresponds to a desorption temperature of only 473K, which is far below the unfavorable desorption temperature of 573 K of bulk MgH_2. Therefore, first principles DFT calculations confirm that nanocrystalline materials possess excellent hydrogen storage properties in theoretical aspect.

For cubic Mg_2NiH_4, the hydrogen atom positions has not been completely determined by diffraction methods due both to the incompatibility of the NiH_4 unit with the cubic space group *Fm-3m* and to the relationship between the neutron scattering lengths for Mg and Ni. García et al [10] performed ab initio total-energy calculation on electronic structure of cubic Mg_2NiH_4 for different hydrogen configurations and concluded that the minimum-energy configuration corresponded to a tetrahedrally distorted square-planar distribution of hydrogen atoms around the nickel atom.

For monoclinic Mg_2NiH_4, Jasen et al [73] calculated its electronic structure and indicated that the hydrogen atoms presented a bonding much more developed with Ni than with Mg and the principal bonding interaction was Ni *sp* - H *s*. Van Setten et al [74] studied the effects of transition metal doping by first principles density functional theory calculations. They indicated that the hydrogen desorption enthalpy could be reduced by ~0.1 eV/H_2 if one in eight Ni atoms was replaced by Cu or Fe and that Cu was the most promising candidate to lower the hydrogen desorption enthalpy of Mg_2NiH_4, which could provide a theoretical guide for selecting appropriate metals to

perform substitutional doping in experimental synthesis.

We have investigated the substitutional doping of Mn in Mg_2Ni phase and the electronic structure of Mg_3MnNi_2 phase by first principles calculations [75]. The calculation of enthalpy of formation showed that among the four different lattice sites of Mg (*6f*), Mg (*6i*), Ni (*3b*) and Ni (*3d*) in Mg_2Ni unit cell, the most preferable site of substitution of Mn in Mg_2Ni lattice has been confirmed to be Mg (*6i*) lattice site. Analysis of density of states (DOS) indicated that there was a strong hybridization between Mg *s*, Mg *p* and Ni *d* electrons, which was dominant in controlling the structural stability of pure and Mn-dope Mg_2Ni phases. The Mn substitution in Mg_2Ni unit cell weakened the interaction between Mg *s*, Mg *p* and Ni *d* electrons. The cubic Mg_3MnNi_2 phase possesses a strong hybridization between Mn and Mg, Ni orbits under simultaneously retaining the strong bonding among Mg *s*, Mg *p* and Ni *d* electrons. As a result, the stability of phases gradually decreased along the sequence pure Mg_2Ni phase > Mg_3MnNi_2 phase > Mn-substitution doped Mg_2Ni phase.

6. Conclusions

Fundamental data on Mg-Ni-based systems and their hydrides, such as phase diagrams, crystal structures and thermodynamical properties etc. are the base for developing Mg-Ni-based hydrogen storage alloys. Amorphous and nanostructured phases in Mg-Ni-based systems are favourable for improving hydrogen storage properties.

Partial elements substitution has been proved to be appropriate for improving hydrogen storage properties of Mg-Ni-based alloys. Exploring new Mg-Ni-based hydrogen storage alloys is significant for developing hydrogen storage technology. Partial elements substitution is expected to change the alloy composition and synthesize new hydrogen storage alloys.

Adding appropriate catalysts can improve the hydriding/dehydriding kinetics of Mg-Ni-based alloys. The mechanism of the catalysis may be caused by a spillover effect, namely dissociative chemisorption of H_2 on a metal and subsequent migration or surface diffusion of the atomic hydrogen onto the support surfaces. Pd is one of the most important catalysts.

Carbon materials, such as graphite, fullerene, activated carbon, carbon black and

CNTs have shown positive effects on the hydrogen storage properties of Mg-Ni-based systems. Therefore, carbon materials addition is promising for ameliorating the hydrogen storage properties of Mg-Ni-based alloys.

Preparing methods play an important role in Mg-Ni-based alloys. The preparing methods that can substantially decrease particle and crystal size, introduce numbers of grain boundaries and defects should be preferential choices.

First principles calculations could explain the experimental results and provide a guide for selecting appropriate substitutional elements. Combined experiment and first principles calculation is quite necessary for screening and discovering novel Mg-Ni-based hydrogen storage materials.

References

[1] Kohno T, Tsuruta S, Kanda M. J Electrochem Soc 1996;143: L198–9.

[2] Reilly JJ, Wiswall RH. Inorg Chem 1968; 7:2254–6.

[3] Schefer J, Fischer P, Hälg W, Stucki F, Schlapbach L, Didisheim JJ, Yvon K, Andresen AF. J Less-Common Met 1980;74:65–73.

[4] ASM International, Binary Alloy Phase Diagrams, Second Edition Plus Updates,1996.

[5] Selvam P, Viswanathan B, Swamy CS, Srinivasan V. Thermochim Acta 1988;125:1–8.

[6] Liu FJ, Sandrock G, Suda S. Z Phys Chem 1994;183 : 163–7.

[7] Orimo S, Seto H, Ikeda K, Nagao M, Fujii H. Physica B 1996;226:370–4.

[8] Zolliker P, Yvon K, Jorgensen JD, Rotella FJ. 1986;25:3590–3.

[9] Yvon K, Schefer J, Stucki F. Inorg Chem 1981;20:2776–8.

[10] García GN, Abriata JP, Sofo JO. Phys Rev B 1999;59:11746–54.

[11] Lupu D, Sârbu R, Biriş A, Lupu D, Sârbu R, Biriş A. Int J Hydrogen Energy 1987;12:425–6.

[12] Schlapbach L, Züttel A. Nature 2001;414: 353–8.

[13] Griessen R. Phys Rev B 1983; 27 : 7575–82.

[14] Batalla E, Ström-Olsen JO, Altounian Z, Boothroyd D, Harris R. J Mater Res 1986;1:765.

[15] Bowman JRC. Mater Sci Forum 1988;31 : 197.

[16] Hayashi S, Orimo S, Fujii H. J Alloys Compd 1997;261:145–9.

[17] Orimo S, Fujii H. Appl Phys A 2001;72:167–86 .

[18] Huang LW, Elkedim O, Jarzebski M, Hamzaoui R, Jurczyk M. Int J Hydrogen Energy 2010;35:6794–803.

[19] Yamamoto K, Fujikawa Y, Ikeda K, Orimo S, Fujii H, Kitano Y. J Electron Microsc 1998;47:461–70.

[20] Xue JS, Li GX, Hu YQ, Du J, Wang CQ, Hu GY. J Alloy Compd 2000;307:240–4.

[21] Wang LB, Wang JB,Yuan, HT, Wang YJ, Li QD. J Alloy Compd 2004;385:304–8.

[22] Lü GL, Chen LS, Wang LB ,Yuan HT. J Alloy Compd 2001;321:L1–4.

[23] Liang G, Huot J, Boily S, Van Neste A, Schulz R. J Alloy Compd 1999;282:286–90.

[24] Ruggeri S, Roué L, Huot J ,Schulz R, Aymard L, Tarascon JM. J Power Sources 2002;112:547–56.

[25] Zhang YH, Han XY, Li BW, Ren HP, Dong XP, Wang XL. J Alloy Compd 2008;450:208–14.

[26] Nohara S, Hamasaki K, Zhang SG, Inoue H, Iwakura C. J Alloy Compd 1998;280:104–6.

[27] Anik M, Akay I, Özdemir G, Baksan B. Int J Hydrogen Energy 2009;34:9765–72.

[28] Zhang Y, Lei YQ, Chen LX, Yuan J, Zhang ZH, Wang QD. J Alloy Compd 2004;337:296–302.

[29] Iwakura C, Shin-ya R, Miyanohara K, Nohara S, Inoue H. Electrochim Acta 2001;46:2781–6.

[30] Jurczyk M, Smardz L, Szajek A. Mater Sci Eng B 2004;10: 67–75.

[31] Gasiorowski A, Iwasieczko W, Skoryna D, Drulis H, Jurczyk M. J Alloys Compd 2004;364: 283–8.

[32] Kohno T, Kanda M. J Electrochem Soc 1997;144: 2384–8.

[33] Ren HP ,Zhang YH, Li BW, Zhao DL, Guo SH, Wang XL. Int J Hydrogen Energy

2009;34:1429–36.
[34] Drenchev N, Spassov T, Kanazirski I . J Appl Electrochem 2008;38:197–202.
[35] Li Q , Jiang LJ, Chou KC, Lin Q, Zhan F, Xu KD, Lu XG, Zhang JY. J Alloy Compd 2005;339:101–5.
[36] Xue JS, Wang LJ, Luo YH, Li GX, Du J, Hu GY, Wang CQ. Rare Metals 2003;22:144–9.
[37] Denys RV, Saldan IV, Delaplane RG, Berezovets VV, Zavaliy IY. IX International Conference on Hydrogen Materials Science & Chemistry of Carbon Nanomaterials, Sevastopol, Ukraine, 2005, pp. 152.
[38] Dobrovolsky VD, Ershova OG, Solonin YM. in: Baranowski B, Zaginaichenko SY, Schur DV, Skorokhod VV, Veziroglu A (Eds.), Carbon Nanomaterials in Clean Energy Hydrogen Systems, Springer, Netherlands, 2008, pp. 467–72.
[39] Hsu F, Lin C, Lee S, Lin C, Bor H. J Power Sources 2010;195:374–9.
[40] PDF No. 00-057-0388, International Centre for Data Diffraction.
[41] Denys RV, Riabov AR, Berezovets VV, Koval'chuk IV, Černý R, Yu Zavaliy I. Intermetallics 2011;19:1563–6.
[42] Zhang YH, Li BW, Ren HP, Guo SH, Zhao DL, Wang XL. Mater Chem Phys 2010;124:795–802.
[43] Zhang, YH, Ren HP, Li BW, Guo SH, Pang ZG, Wang XL. Int J Hydrogen Energy 2009;34:8144–51.
[44] Wang MH, Zhang Y, Zhang LZ, Sun LX, Tan ZC, Xu F, Yuan HT, Zhang T. J Power Sources 2006;159:159-62. Wang MH, Zhang LZ, Zhang Y, Sun LX, Tan ZC, Xu F, Yuan HT, Zhang T. Int J Hydrogen Energy 2006;31:775–9.
[45] Robell AJ, Ballou E V, Boudart M. J Phys Chem 1964;68: 2748–53.
[46] Conner W C, Falconer J L. Chem Rev 1995;95: 759–88.
[47] Gross KJ, Chartouni D, Leroy E, Züttel A, Schlapbach L. J Alloys Compd 1998;269:259–70.
[48] Gutfleisch O, Schlorke-de Boer N,Ismail N, Herrich M, Walton A, Speight J, Harris IR,Pratt AS, Züttel A. J Alloys Compd 2003;356-357:598–602.
[49] Zaluski L, Zaluska A, Tessier P, Ström-Olsen JO, Schulz R. J Alloys Compd 1995;217:295–300.
[50] Xu XC, Song CS. Appl Catal A-Gen 2006;300:130–8.
[51] Adelhelm P, de Jongh PE. J Mater Chem 2011;21: 2417–27.
[52] Bouaricha S, Dodelet JP, Guay D, Huot J, Boily S, Schulz R. J Alloys Compd 2000;307: 226–33.
[53] Wu CZ, Wang P, Yao X, Liu C, Chen DM, Lu GQ, Cheng HM. J Alloys Compd 2006;414: 259–64.
[54] Amirkhiz BS, Danaie M, Mitlin D. Nanotechnology 2009; 20: 204016.
[55] Amirkhiz BS, Danaie M, Barnes M, Simard B, Mitlin D. J Phys Chem C 2010;114:3265–75.
[56] Pandey SK, Singh RK, Srivastava ON. Int J Hydrogen Energy 2009;34:9379–84.
[57] Aminorroaya S, Liu HK, Cho Y, Arne Dahle. Int J Hydrogen Energy 2010;35:4144–53.
[58] Verón MG, Troiani H, Gennari FC. Carbon 2011; 49:2413–23.
[59] Huang LW, Elkedim O, Nowak M, Jurczyk M, Chassagnon R, Meng DW. Int J Hydrogen Energy 2012;37:1538–45.

[60] Suryanarayana C. Progr Mater Sci 2001;46: 1–184.
[61] Yim CD, You BS, Na YS, Bae JS. Catal Today 2007;120:276–80.
[62] Zaluski L, Zaluska A, Ström-Olsen JO. J Alloys Compd 1995;217:245–9.
[63] Budhani RC, Goel TC, Chopra KL. Bull Mater Sci1982; 4:549–61.
[64] Zhang, YH, Ren HP, Li BW, Guo SH, Pang ZG, Wang XL. Int J Hydrogen Energy 2009;34:8144–51.
[65] Zhang YH, Li BW, Ren HP, Guo SH, Zhao DL, Wang XL. Mater Chem Phys 2010;124:795–802.
[66] Akiyama T, Isogai H, Yagi J. J Alloys Compd 1997;252:L1–4.
[67] Liu DM, Zhu YF, Li LQ. Int J Hydrogen Energy 2007;32:2455–60.
[68] Liu XF, Zhu YF, Li LQ. J Alloy Compd 2006;425:235–8.
[69] Liu XF, Zhu YF, Li LQ. Int J Hydrogen Energy 2007;32:2450–4.
[70] Ikeda Y, Ohmori T. Int. J. Hydrogen Energy 2009;34 : 5439–5443.
[71] Kumar LH, Viswanathan B, Murthy SS. J. Alloys Compd 2008;461: 72–76.
[72] Wagemans RWP, van Lenthe JH, de Jongh PE, van Dillen AJ, de Jong KP. J Am Chem Soc 2005; 127:16675–80.
[73] Jasen P V, Gonzalez EA, Brizuela G, Nagel O A, González GA, Juan A. Int J Hydrogen Energy 2007;32 :4943 –8.
[74] van Setten M J, de Wijs GA, Brocks G. Phys. Rev. B 76 (2007) 075125.
[75] Huang LW, Elkedim O, Hamzaoui R. J Alloys Compd 2011;509S :S328–33.

ANNEXE 2

Huang LW, Elkedim O, Moutarlier V. Synthesis and characterization of nanocrystalline Mg_2Ni prepared by mechanical alloying: Effects of substitution of Mn for Ni. Journal of Alloys and Compounds 2010 ; 504 : S311–4.

Journal of Alloys and Compounds 504S (2010) S311–S314

Contents lists available at ScienceDirect

Journal of Alloys and Compounds

journal homepage: www.elsevier.com/locate/jallcom

Synthesis and characterization of nanocrystalline Mg_2Ni prepared by mechanical alloying: Effects of substitution of Mn for Ni

L.W. Huang[a,*], O. Elkedim[a], V. Moutarlier[b]

[a] FEMTO-ST, MN2S, Université de Technologie de Belfort-Montbéliard, Site de Sévenans, 90010 Belfort cedex, France
[b] Institut UTINAM, UMR 6213, 16 Route de Gray, 25000 Besançon, France

ARTICLE INFO

Article history:
Received 3 July 2009
Received in revised form 4 January 2010
Accepted 10 February 2010
Available online 18 February 2010

Keywords:
Mg_2Ni alloy
Mn
Mechanical alloying
Nanocrystalline
Elemental substitution

ABSTRACT

The $Mg_2Ni_{(1-x)}Mn_x$ ($x = 0, 0.125, 0.25, 0.375$) hydrogen storage alloys have been synthesized by mechanical alloying (MA). The effects of substitution of Mn for Ni on the phase composition and microstructures of Mg_2Ni-type alloys have been investigated by X-ray diffraction (XRD) and scanning electron microscopy (SEM). XRD results of milled samples indicate that substitution of Mn for Ni could inhibit the formation of $MgNi_2$ phase and the solid solubility of Mn in Mg_2Ni phase is low. The calculation of average crystallite size and microstrain of $Mg_2Ni_{(1-x)}Mn_x$ alloys milled for 8 h shows that with the increase of substitution amount of Mn for Ni from $x = 0$ to $x = 0.375$, the average crystallite size decreases first from 12.5 nm to 9.6 nm and then increases from 9.6 nm to 11.8 nm with the minimum 9.6 nm obtained at $x = 0.25$, while the microstrain monotonously decreases from 1.39% to 0.82%. SEM has revealed that the sizes of subparticles that constitute the powder particles in the composition $Mg_2Ni_{0.75}Mn_{0.25}$ are much smaller than those in other compositions.

1. Introduction

Many intermetallic compounds are attractive candidates for hydrogen storage due to their capability of reversibly absorbing large amounts of hydrogen. If AB_n ($n = 0.5, 1, 2, 5$) is used to denote the binary intermetallic compounds for hydrogen storage, element A is usually a rare earth (e.g. La), an alkaline earth metal (e.g. Mg) or former transition metal (e.g. Ti, Zr) and tends to form a highly stable hydride at room temperature. Whereas element B is often a latter transition metal (e.g. Fe, Ni, Cu) and does not form stable hydrides at room temperature [1–3]. The combination of different elements in AB_n can be used to design and tailor the properties, such as Mg_2Ni [4], TiFe [5], ZrV_2 [6] and $LaNi_5$ [7]. Mg_2Ni intermetallic compound is one of the most promising alloys in the AB_n family, since besides its lightweight and low cost, its theoretical gravimetric storage hydrogen capacity, assuming the formation of Mg_2NiH_4, is 3.6 mass% (equivalent to 999 mAh/g for the discharge capacity, which is approximately 2.7 times that of $LaNi_5$) and it can absorb and desorb hydrogen at more moderate temperatures and pressures than other alloys. However, the poor hydriding/dehydriding kinetics and high thermodynamical stability of Mg_2NiH_4 (requiring 280 °C for 1 bar hydrogen [8]) become the obstacle for the practical use for hydrogen storage.

There are many methods to improve the hydrogen storage properties or electrochemical hydrogen storage properties of Mg_2Ni intermetallic compound: (a) adding suitable catalysts [4,9]; (b) increasing specific surface area [10]; (c) substituting partial elements [11–13] and (d) using new synthesis methods to decrease the crystallite size to nanoscale (such as mechanical alloying [4], polyol reduction method [14]). Mechanical alloying (MA) is a solid-state powder processing technique involving repeated welding, fracturing, and rewelding of powder particles in a high-energy ball mill [15]. This method is considered to be more appropriate for synthesizing Mg_2Ni intermetallic compound than conventional metallurgical methods, such as melting, because of the low miscibility of Mg with most transition metals, the high vapor pressure of Mg and the difference between Mg and Ni melting points. Nanocrystalline Mg_2Ni produced by MA showed substantially enhanced absorption and desorption kinetics, even at relatively low temperatures [16].

Yang et al. [17] found that replacement of Ni in Mg_2Ni by Mn lowered the decomposition plateau pressure. Kohno and Kanda [18] reported that as a result of substitution of Mg with Mn, absorption of hydrogen occurred at lower temperature. Gasiorowski et al. [12] found that the partial substitution of Mg by Mn in Mg_2Ni alloy leaded to an increase in discharge capacities at room temperature. It can be seen that different authors used different substitution methods. Some used Mn to substitute Ni, while others used Mn to substitute Mg in Mg_2Ni. Tsushio and Akiba [19] proposed that for designing a quaternary alloy system of Mg_2Ni by substitution

* Corresponding author.
E-mail address: liwu.huang@utbm.fr (L.W. Huang).

0925-8388/$ – see front matter © 2010 Elsevier B.V. All rights reserved.
doi:10.1016/j.jallcom.2010.02.059

Table 1
Phase composition of $Mg_2Ni_{(1-x)}Mn_x$ (x = 0, 0.125, 0.25, 0.375) alloys for different milling times.

Sample	Phase composition			
	4 h	8 h	16 h	24 h
Mg_2Ni	Mg, Ni, traces of Mg_2Ni	Mg_2Ni, $MgNi_2$	Mg_2Ni, $MgNi_2$	Mg_2Ni, $MgNi_2$
$Mg_2Ni_{0.875}Mn_{0.125}$	Mg, Ni, Mn	Mg_2Ni, Mn, traces of $MgNi_2$	Mg_2Ni, Mn, traces of $MgNi_2$	Mg_2Ni, Mn, traces of $MgNi_2$
$Mg_2Ni_{0.75}Mn_{0.25}$	Mg, Ni, Mn	Mg_2Ni, Mn	Mg_2Ni, Mn	Mg_2Ni, Mn
$Mg_2Ni_{0.625}Mn_{0.375}$	Mg, Ni, Mn	Mg_2Ni, Mn	Mg_2Ni, Mn	Mg_2Ni, Mn

method, the substitution for Ni had to be considered first and then for Mg. However, the literatures that reported using the different substitution ratios of Mn for Ni in Mg_2Ni alloy to study the effects are few.

The purpose of this work is to synthesize the $Mg_2Ni_{(1-x)}Mn_x$ (x = 0, 0.125, 0.25, 0.375) alloys by MA and to investigate the effects of substitution of Mn for Ni on the phase composition and microstructures of Mg_2Ni-type alloys systematically for providing a guide for improving the hydrogen storage properties of Mg_2Ni intermetallic compound.

2. Experimental procedure

Starting elemental powders of Mg (purity 99.8%, particle size ≤50 μm, from GoodFellow), Ni (purity 99.5%, particle size ≤250 μm, from GoodFellow) and Mn (particle size −325 mesh, purity 99.3%, from Alfa) were mixed and poured into the stainless steel vials (volume 50 ml) together with two stainless steel balls (diameter 20 mm) in the glove box filled with argon according to the designed composition $Mg_2Ni_{(1-x)}Mn_x$ (x = 0, 0.125, 0.25, 0.375). The MA was carried out with 20:1 ball to powder weight ratio under argon atmosphere at room temperature using a planetary high-energy ball mill (Retsch PM 400) at a speed of 400 rpm. The milling was interrupted for 30 min/h to dissipate the heat and to reduce the excessive rise of temperature.

The structures of the MA alloys with different compositions milled for different periods of time were analyzed by the Bruker D8 Advance X-ray diffractometer with Cu Kα radiation (λ = 0.15418 nm) filtered by nickel. The crystallite size and microstrain were calculated from the approximation (Eq. (1)) that combines the Wilson formula and Scherrer formula following Williamson–Hall style plot [20].

$$\beta = 2\varepsilon \tan\theta + \frac{0.9\lambda}{d\cos\theta} \quad (1)$$

where β is the full-width at half maximum intensity of a Bragg reflection excluding instrumental broadening, θ the Bragg angle, λ the wavelength of the X-ray radiation, ε the effective lattice microstrain and d the average crystallite size.

The morphologies of the powdered samples were observed using the JEOL JSM-5800LV Scanning Electron Microscope.

3. Results and discussion

Fig. 1 shows the evolution of X-ray diffraction patterns of $Mg_2Ni_{(1-x)}Mn_x$ (x = 0, 0.125, 0.25, 0.375) alloys mechanically alloyed for 8 h. It can be seen that all MA alloys exhibit new diffraction peaks, which are identified as Mg_2Ni or $MgNi_2$ phase. The Mg_2Ni phase exists in all composition, whereas $MgNi_2$ phase gradually decreases with the increase of x (the content of Mn) and disappears as x achieves 0.25 and 0.375. Phase composition of $Mg_2Ni_{(1-x)}Mn_x$ (x = 0, 0.125, 0.25, 0.375) alloys for different milling times is displayed in Table 1. This phenomenon indicates that substitution of Mn for Ni could inhibit the formation of $MgNi_2$ phase, which is possibly ascribed to the change of atom ratios between Mg and Ni. During mechanical alloying, since Mg is very soft and easier to adhere to the balls and walls of vials, the real content of Ni is above and near to 33 at% for x = 0 and x = 0.125 (smaller amount of substitution), respectively, which is corresponding to the $Mg_2Ni + MgNi_2$ region in the Mg–Ni system. Therefore, Mg_2Ni and small amount of $MgNi_2$ phases coexist for x = 0 and 0.125. After large amount of substitution of Mn for Ni, Ni content is below 33 at%, which belongs to the $Mg_2Ni + Mg$ region. As a result, $MgNi_2$ phase disappears when x = 0.25 and 0.375. In contrast to Mg_2Ni, the $MgNi_2$ phase does not interact with hydrogen [21], so the substitution of Mn for Ni is favorable for synthesizing the single Mg_2Ni phase and improve the hydrogen storage capacity by promoting the reaction of Mg and Ni to form Mg_2Ni phase. It is also noted that the peaks of Mn phase still exist in Fig. 1(c)–(e), meaning that it is difficult for Mn to enter into the lattice of Mg_2Ni phase, which is also reported in Ref. [22]. This phenomenon is probably explained as follows. Electronegativities of metal elements gradually increase along the sequence Mg < Mn < Ni. Therefore, due to the bigger difference of electronegativities between Ni and Mg in comparison with Mn, it is much easier for bonding between Mg and Ni. As a result, it is difficult for Mn to substitute the site of Ni in Mg_2Ni lattice. Fig. 2 shows X-ray diffraction patterns of the $Mg_2Ni_{0.25}Mn_{0.75}$ alloys with different milling times. After 4 h of milling, the intensities of the diffraction peaks of Mg, Ni and Mn decrease and their peak widths increase as a result of the reduction of crystallite size and/or the accumulation of microstrain during MA. When milling duration is 8 h, the peaks of Mg_2Ni phase appear, while the peaks of Mg and Ni nearly disappear. Although the milling time is prolonged to 24 h, there are still the Mn peaks of high intensity, which further proves the solid solubility of Mn in Mg_2Ni phase is low.

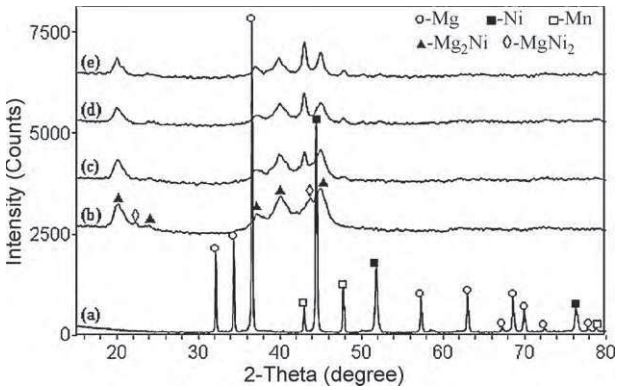

Fig. 1. X-ray diffraction patterns of the initial elemental powder mixture (a) and the $Mg_2Ni_{(1-x)}Mn_x$ alloys with a fixed milling time of 8 h: (b) x = 0, (c) x = 0.125, (d) x = 0.25 and (e) x = 0.375.

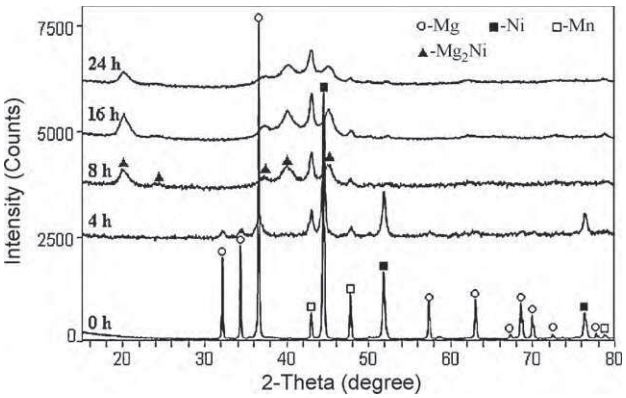

Fig. 2. X-ray diffraction patterns of the initial elemental powder mixture (0 h) and the $Mg_2Ni_{0.25}Mn_{0.75}$ alloys with different milling times.

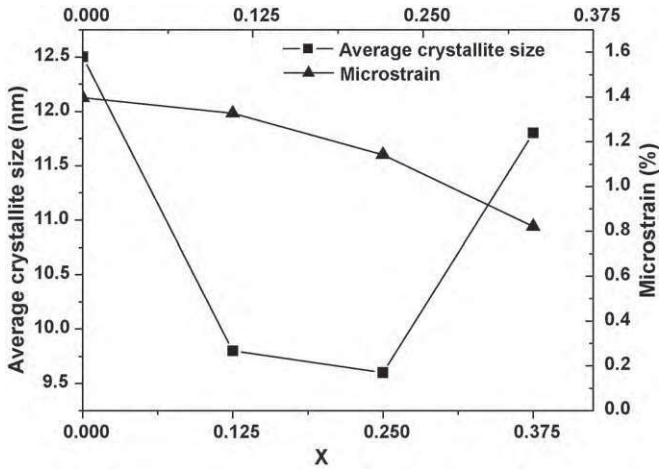

Fig. 3. Evolution of average crystallite size and microstrain of $Mg_2Ni_{(1-x)}Mn_x$ ($x = 0$, 0.125, 0.25, 0.375) alloys milled for 8 h versus x.

X-ray diffraction peak broadening shown in Fig. 1 is evaluated and the evolution of average crystallite size and microstrain for different substitution amounts of Mn for Ni is presented in Fig. 3. It is observed that within a fixed milling time (8 h), with the increase of substitution amount of Mn for Ni from $x = 0$ to $x = 0.375$, the average crystallite size decreases first from 12.5 nm to 9.6 nm and then increases from 9.6 nm to 11.8 nm with the minimum 9.6 nm obtained at $x = 0.25$, while the microstrain monotonously decreases from 1.39% to 0.82%. This result may be explained as follows. Both Mg and Ni are malleable and ductile, while Mn is hard and brittle. With the increase of substitution amount of Mn for Ni, the hardness and brittleness of MA powders substantially increase, which is favorable for the MA powders to get work hardened and causes more intensive collisions among powders, resulting in more easily fracturing of crystal grains. Therefore, the average crystallite size decreases first with the increase of Mn content from $x = 0$ to 0.25. With the concomitant decline of crystallite size, the grain boundary increases remarkably, which is beneficial to the defects to migrate out of the crystallites, and consequently promotes microstrain release. Additionally, due to the enhancement of brittleness of MA powders, the tendency to fracture predominates over deformation. Because of the fact that the deformation can introduce a great number of defects which can increase microstrain, the weakened tendency to deform leads to the decline of microstrain. As a result, the microstrain decreases with the increase of Mn content from $x = 0$ to 0.25. When the content of Mn increases to a certain extent ($x = 0.375$), the rise of temperature caused by more intensive collisions cannot be ignored and consequently accelerates the crystal grains growth and the lattice strain release, which is the probable reason why the crystallite size increases from 9.6 nm to 11.8 nm and the microstrain decreases from 1.14% to 0.82% for $Mg_2Ni_{0.625}Mn_{0.375}$ in comparison with that of $Mg_2Ni_{0.75}Mn_{0.25}$. Orimo and Fujii [1] reported that the average crystallite sizes of Mg_2Ni alloy reduced down to nearly 16 nm by milling for 3.6 ks according to the peak broadening of the X-ray diffraction profiles using Wilson method [23]. Due to using longer milling time (8 h) in this study compared with 3.6 ks, smaller average crystallite size (12.5 nm) is obtained for Mg_2Ni. MA is proved to strongly promote the formation of Mg_2Ni. In fact, traces of Mg_2Ni has already appeared after only 4 h of milling for $x = 0$ (Table 1). After formation of Mg_2Ni, the tendency to fracture is reinforced because of the brittle behavior of ordered intermetallic structures [24]. This is also supported by the phenomenon that the collisions noise began to rise after 3 h of milling, which reveals that the sample powder has become much harder. As a result, repeated strong ball-powder collisions significantly introduce the microstrain and cause the reduction of crystallite size. The induced microstrain can assist diffusion by reducing the hysteresis of hydrogen absorption and desorption [25]. The formation of nanocrystalline Mg_2Ni gives an

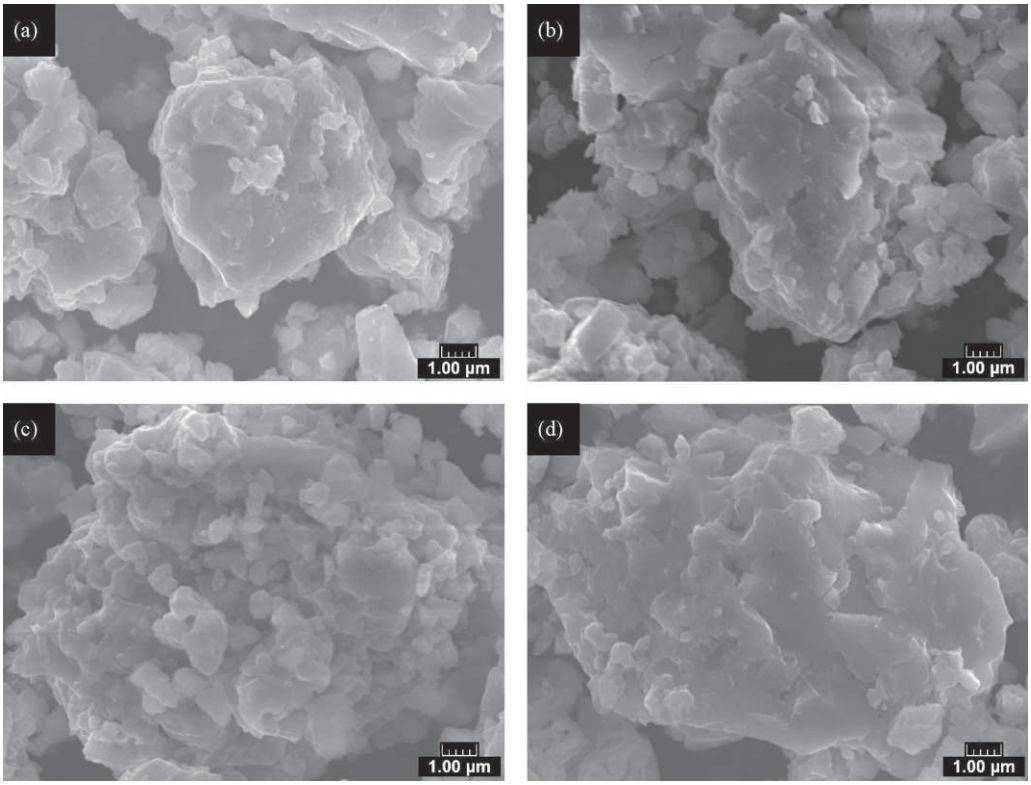

Fig. 4. SEM morphologies of the $Mg_2Ni_{(1-x)}Mn_x$ alloys with a fixed milling time of 8 h: (a) $x = 0$, (b) $x = 0.125$, (c) $x = 0.25$ and (d) $x = 0.375$.

enormously increased amount of grain boundaries which can provide easier channel for the diffusion of hydrogen atoms. At the same time, nanoscale Mg_2Ni alloy can avoid the long-range diffusion of hydrogen atoms through the already formed hydride phase [16]. So the hydriding/dehydriding kinetics can be improved due to the introduction of microstrain and reduction of crystallite size.

Fig. 4 shows the SEM morphologies of the $Mg_2Ni_{(1-x)}Mn_x$ ($x = 0$, 0.125, 0.25, 0.375) alloys with a fixed milling time of 8 h. It is observed that the powder particles in all the compositions are mainly flaky and show cleavage fracture morphology and inhomogeneous size distribution, which is the same as that observed by Gasiorowski et al. [12]. The powder particles are also agglomerates of many smaller particles (namely subparticles), which is because a large amount of energy of balling is transferred to particles, resulting in high concentration of defects and decrease of particle size, which increases the surface free energy of particles. In order to decrease the total energy of particles, subparticles agglomerate together to reduce the surface area for lowering surface free energy. The size of agglomerates shows the tendency of increase with the increase of x from 0 (Fig. 4(a)) to 0.375(Fig. 4(d)) excluding $x = 0.25$. It is noteworthy that the subparticles that constitute powder particles in Fig. 4(c) are much smaller than those in Fig. 4(a), (b) and (d). This is because with the increase of Mn content, the hardness and brittleness of MA powders increase, which is favorable for the particles to fracture. As a result, the subparticle sizes decrease when x increases from 0 to 0.25. Whereas, as mentioned above, excessive Mn ($x = 0.375$) enhances the collisions among particles, resulting in the substantial rise of temperature, which promotes the welding that tends to increase the particle size. As a result, the subparticle sizes rebound when x increases from 0.25 to 0.375. Therefore, there exist an optimal value of Mn content for obtaining smallest subparticles, namely $x = 0.25$. The smaller size of subparticles in Fig. 4(c) will significantly increase the surface area of the powder particles compared with the bigger ones in Fig. 4(a), (b) and (d), which will facilitate the absorption of hydrogen at the surface of Mg_2Ni alloy and improve the hydrogen storage properties of Mg_2Ni intermetallic compound. Yang et al. [17] measured the specific surface areas of $Mg_2Ni_{0.75}Mn_{0.25}$ and Mg_2Ni alloys and got the value of 3.9 m^2/g for $Mg_2Ni_{0.75}Mn_{0.25}$ and 3.8 m^2/g for Mg_2Ni, which indicates that substitution of Mn for Ni at $x = 0.25$ is indeed helpful for increasing the specific surface areas of the alloys.

4. Conclusions

Based on this study, the following conclusions can be obtained: (1) substitution of Mn for Ni could inhibit the formation of $MgNi_2$ phase that does not interact with hydrogen; (2) the solid solubility of Mn in Mg_2Ni phase is low; (3) with the increase of substitution amount of Mn for Ni from $x = 0$ to $x = 0.375$, the average crystallite size decreases first from 12.5 nm to 9.6 nm and then increases from 9.6 nm to 11.8 nm with the minimum 9.6 nm obtained at $x = 0.25$, while the microstrain monotonously decreases from 1.39% to 0.82%; (4) SEM morphologies indicate that the powder particles in all the compositions are mainly flaky and show cleavage fracture morphology and inhomogeneous size distribution. The sizes of subparticles of the composition $Mg_2Ni_{0.75}Mn_{0.25}$ are smaller than those of the other compositions, which indicates that the substitution of Mn for Ni at $x = 0.25$ is favorable for the increase of the surface areas of the Mg_2Ni intermetallic compound.

Acknowledgment

The authors would like to thank Mr. O. Rapaud for his technical assistance concerning SEM.

References

[1] S. Orimo, H. Fujii, Appl. Phys. A 72 (2001) 167–186.
[2] A. Züttel, Mater. Today 6 (2003) 24–33.
[3] M. Latroche, J. Phys. Chem. Solids 65 (2004) 517–522.
[4] L. Zaluski, A. Zaluska, J.O. Ström-Olsen, J. Alloys Compd. 217 (1995) 245–249.
[5] C.H. Chiang, Z.H. Chin, T.P. Perng, J. Alloys Compd. 307 (2000) 259–265.
[6] M. Jurczyk, W. Rajewski, G. Wójcik, W. Majchrzycki, J. Alloys Compd. 285 (1999) 250–254.
[7] G. Liang, J. Huot, R. Schulz, J. Alloys Compd. 320 (2001) 133–139.
[8] L. Schlapbach, A. Züttel, Nature 414 (2001) 353–358.
[9] L. Zaluski, A. Zaluska, P. Tessier, J.O. Ström-Olsen, R. Schulz, J. Alloys Compd. 217 (1995) 295–300.
[10] J. Huot, S. Bouaricha, S. Boily, J.-P. Dodelet, D. Guay, R. Schulz, J. Alloys Compd. 266 (1998) 307–310.
[11] Y.H. Zhang, X.Y. Han, B.W. Li, H.P. Ren, X.P. Dong, X.L. Wang, J. Alloys Compd. 450 (2008) 208–214.
[12] A. Gasiorowski, W. Iwasieczko, D. Skoryna, H. Drulis, M. Jurczyk, J. Alloys Compd. 364 (2004) 283–288.
[13] H.T. Yuan, L.B. Wang, R. Cao, Y.J. Wang, Y.S. Zhanga, D.Y. Yan, W.H. Zhang, W.L. Gong, J. Alloys Compd. 309 (2000) 208–211.
[14] L. Hima Kumar, B. Viswanathan, S. Srinivasa Murthy, J. Alloys Compd. 461 (2008) 72–76.
[15] C. Suryanarayana, Prog. Mater. Sci. 46 (2001) 1–184.
[16] L. Zaluski, A. Zaluska, J.O. Ström-Olsen, J. Alloys Compd. 253–254 (1997) 70–79.
[17] H.B. Yang, H.T. Yuan, J.T. Ji, H. Sun, Z.X. Zhou, T.S. Zhang, J. Alloys Compd. 330–332 (2002) 640–644.
[18] T. Kohno, M. Kanda, J. Electrochem. Soc. 144 (1997) 2384–2388.
[19] Y. Tsushio, E. Akiba, J. Alloys Compd. 267 (1998) 246–251.
[20] G.K. Williamson, W.H. Hall, Acta Metall. 1 (1953) 22–31.
[21] M. Terzieva, M. Khrussanova, P. Peshev, J. Alloys Compd. 267 (1998) 235–239.
[22] J. Woo, K. Lee, J. Electrochem. Soc. 146 (1999) 819–823.
[23] H.P. Klug, L.E. Alexander, X-ray Diffraction Procedures—For Polycrystalline and Amorphous Materials, 2nd edn, Wiley-Interscience, New York, 1974, p. 618.
[24] A. Ebrahimi-Purkani, S.F. Kashani-Bozorg, J. Alloys Compd. 456 (2008) 211–215.
[25] G. Liang, E. Wang, S. Fang, J. Alloys Compd. 223 (1995) 111–114.